Chemical Physics 415 (2013) 161–167

Contents lists available at SciVerse ScienceDirect

Chemical Physics

journal homepage: www.elsevier.com/locate/chemphys

Cycloaddition of ozone to allyl alcohol, acrylic acid and allyl aldehyde: A comparative DFT study

Jing Yang [a,*], Jiankui Miao [a], Xuejiao Li [a], Wenguo Xu [b,*]

[a] Department of Chemistry, Tangshan Normal College, Tangshan 063000, PR China
[b] The Key Laboratory of Cluster Science, Ministry of Education of China, School of Science, Beijing Institute of Technology, Beijing 10008, PR China

ARTICLE INFO

Article history:
Received 9 May 2012
In final form 8 January 2013
Available online 17 January 2013

Keywords:
Cycloaddition
Ozone
Allyl alcohol
Acrylic acid
Allyl aldehyde
Rate constant

ABSTRACT

Density functional theory and ab initio methods have been used to calculate the structures and energies of minima and transition sates for the cycloadditions of ozone to allyl alcohol, acrylic acid and allyl aldehyde. The results show that the reactivity of the compounds with respect to addition of ozone to the double bond is a function of the nature of the oxygenated substituents. The acrylic acid is more reactive toward ozone than the corresponding allyl aldehyde, consistent with the relative magnitude of the electron-withdrawing influence of the substituent oxygenated groups. In comparison with acrylic acid and allyl aldehyde, the cycloaddition of ozone to allyl alcohol should be the most favored thermodynamically. Moreover, the calculated rate constants of the three cycloaddition reactions at the BH&HLYP/6-31 + G(d,p) level of theory are in good agreement with experimental data.

1. Introduction

Volatile organic compounds, or VOCs, are an important class of air pollutants, commonly found in the atmosphere at ground level in all urban and industrial centres [1–7]. Field measurements indicate that oxygenated VOCs form a major component of the trace gasses found in the troposphere [8], and hence play an important role in determining the oxidizing capacity of the troposphere both on a regional and a global scale [9]. Oxidation of unsaturated oxygenated compounds in the atmosphere can be initiated by the reaction with ozone [10–13], nitrate and hydroxyl radicals. The reduction of VOCs can be estimated by air quality simulation models such as the regional atmospheric chemistry mechanism (RACM) or the master chemical mechanism (MCM) [14]. In these models, the initial reaction step with ozone involves some unsaturated oxygenated compounds, since they contain unsaturated carbon bonds that are the preferred sites for ozone addition. Unsaturated oxygenated compounds, such as alcohols, aldehydes, and acids et al. are of major importance in the atmosphere, which are present as a result of direct anthropogenic and biogenic emissions [15]. In comparison to the extensive kinetic and mechanistic database available on the gas-phase ozonolysis reactions of alkenes, however, the information on the gas-phase ozonolysis reactions of unsaturated oxygenated compounds is currently limited [16–21]. The reaction mechanisms and reaction rate constants should, as is the case for alkenes [22], vary as a function of the nature of substituents. Therefore, in this paper, allyl alcohol, acrylic acid, and allyl aldehyde are considered as model VOCs to evaluate the effect of different functional groups in the ozonolysis reactions. In this context, thermodynamics and kinetics studies of relevant gas-phase reactions of ozone with these important compounds would assist in understanding their fates in the atmosphere and industry.

The mechanisms of ozonolysis of the alkenes introduced by Criegee [23,24], now widely accepted in literatures, have been proven in a remarkable way: the path for the ozonolysis reaction passes through an O-envelope-shaped van der Waals (VDW) complex and a transition state, and then produces a primary ozonide with a similar structure to the transition state. In this work, transition states for the relatively simple model compounds allyl alcohol, acrylic acid, and allyl aldehyde in their reaction with ozone will be determined and the heights of the reaction barriers will be calculated. A detailed analysis of the geometries of the stationary points on the potential energy surfaces is given. The results are briefly discussed with respect to substituent effects on reactivity. The thermal rate constants of the title reactions are calculated using the conventional transition state theory (TST) [25], the canonical variational transition state theory (CVT) [25–28] coupled with the small-curvature tunneling (SCT) correction (CVT/SCT) [29–31] and the microcanonical variational transition state theory (μVT) [25,32,33] based on the density functional theory calculations.

* Corresponding authors. Fax: +86 0315 3863291.
E-mail address: yjlzddove@tstc.edu.cn (J. Yang).

0301-0104/$ - see front matter © 2013 Elsevier B.V. All rights reserved.
http://dx.doi.org/10.1016/j.chemphys.2013.01.005

2. Calculation methods

2.1. Electronic structure calculations

Earlier studies have shown that the hybrid Hartree–Fock density-functional method, abbreviated HDFT, can provide reasonably accurate prediction of the information along the reaction path. In this study, the geometries and frequencies of all stationary points (reactants, transition states and the primary ozonides) are optimized using the BH&HLYP method in conjunction with 6-31 + G(d,p) basis set that was also demonstrated to be an effective basis set in Truhlar et al.'s study [34]. Synchronously, to validate the reliability of the BH&HLYP method, the same calculations are performed by MPWB1K [35,36] and MPW1K [37–39] methods with the same basis set. The graphical representations of all stationary points for the title reactions are depicted in Figs. 1–3, respectively. Single-point energy calculations are performed at the CCSD(T)/6-31 + G (df,p) level of theory based on BH&HLYP-optimized geometries. The minimum energy paths (MEPs) from $s = -1.50$–1.50 amu$^{1/2}$ bohr are done in the mass weighted Cartesian coordinate with a step size of 0.01 amu$^{1/2}$ bohr, using the intrinsic reaction coordinate (IRC) method at three DFT levels of theory. Along this energy path, the reaction coordinate s is defined as the signed distance from the saddle point, with $s > 0$ referring to the product side. At 20 selected points (selected by a focusing technique [40]) along the MEP, the force constant matrixes as well as the harmonic vibrational frequencies are calculated at the same levels of theory. Furthermore, the energies of the selected points are refined by the CCSD(T) method. In addition, the method of natural bond orbital (NBO) analysis [41] has been used to study the orbital interactions as well as the electronic structure of these compounds at the BH&HLYP/6-31 + G(d,p) level. The calculated absolute energies, harmonic frequencies, and zero-point energies of the molecules considered in this work are given in the Supporting Information (Tables 1S and 2S). All the above calculations are performed using the Gaussian 03 [42] program.

2.2. Rate constant calculations

The conventional transition state theory, the canonical variational transition state theory, and the microcanonical variational transition state theory are employed to calculate the rate constants for the two bimolecular reactions. There exists the considerable literatures on the TST, CVT and μVT formalisms. Below, we give only a brief description of them, which has been implemented in the Vklab 1.0 [43] programs.

Within the transition-state theory (TST) [25] framework, thermal rate constants of a reaction can be expressed as

$$K(T) = \kappa(T)\sigma\frac{k_B T}{h}\frac{Q^{\neq}(T)}{\Phi^R(T)}e^{\{-\Delta V^{\neq}/k_B T\}}$$

where κ is the transmission coefficient accounting for the quantum mechanical tunneling effects; σ is the reaction symmetry number; $Q^{\neq}$ and Φ^R are the total partition functions (per unit volume) of the transition state and reactants, respectively; $\Delta V^{\neq}$ is the classical barrier height; T is the temperature; k_B and h are the Boltzmann and Plank constants, respectively.

The variational transition state rate constant for a gas-phase bimolecular reaction is determined by varying the location of the dividing surface along a reference path to minimize the rate constant at a given temperature. In other words, CVT minimizes the recrossing effects by effectively moving the dividing surface along the minimum energy path (MEP) so as to minimize the rate constant. In the present study, the MEP is defined as the steepest descent path from the saddle point to both the reactant and product sides in the mass-weighted Cartesian coordinate system. The reaction coordinate, s, is defined as the distance along the MEP with the origin located at the saddle point and is positive on the product side and negative on the reactant side. For a canonical ensemble at a given temperature T, the canonical variational transition state theory (CVT) [26–28] thermal rate constant $k^{CVT}(T)$ is given by

$$k^{CVT}(T) = \min_s k^{GT}(T,s)$$

where

$$k^{GT}(T,s) = \left\{\sigma\frac{k_B T}{h}\frac{Q^{GT}(T,s)}{\Phi^R(T)}e^{-V_{MEP}(s)/k_B T}\right\}$$

where $k^{GT}(T,s)$ is the generalized transition state theory rate constant at the dividing surface which intersects the MEP at s and is orthogonal to the MEP. Here, σ is the symmetry factor accounting for the possibility of more than one symmetry-related reaction path, k_B is Boltzman's constant and h is Plank's constant. Q^{GT} is the internal partition function of the generalized transition state with the local zero of energy at $V_{MEP}(s)$. Φ^R is the reactant partition

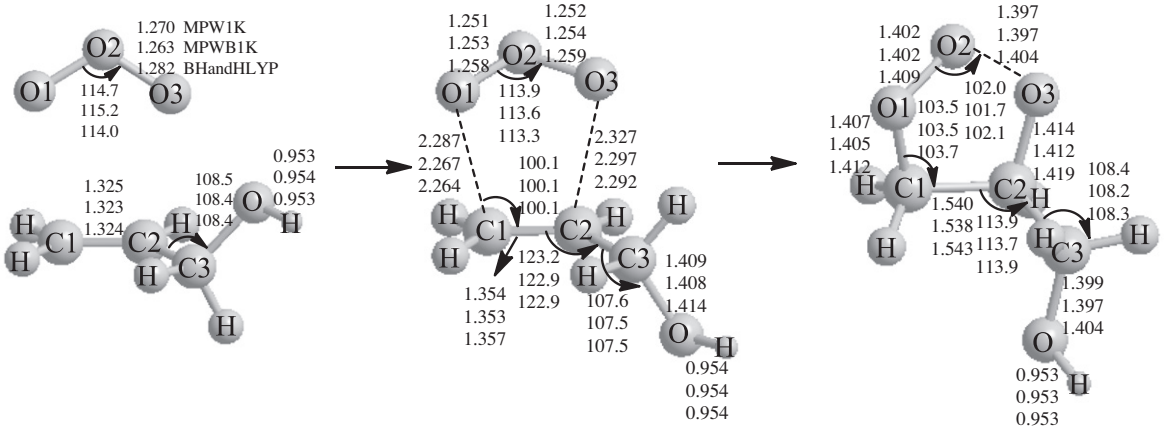

Fig. 1. Cycloaddition of ozone on allyl alcohol: Optimized BH&HLYP, MPWB1K and MPW1K geometries of the stationary points. Angles are given in degree, and bond distances are given in angstroms.

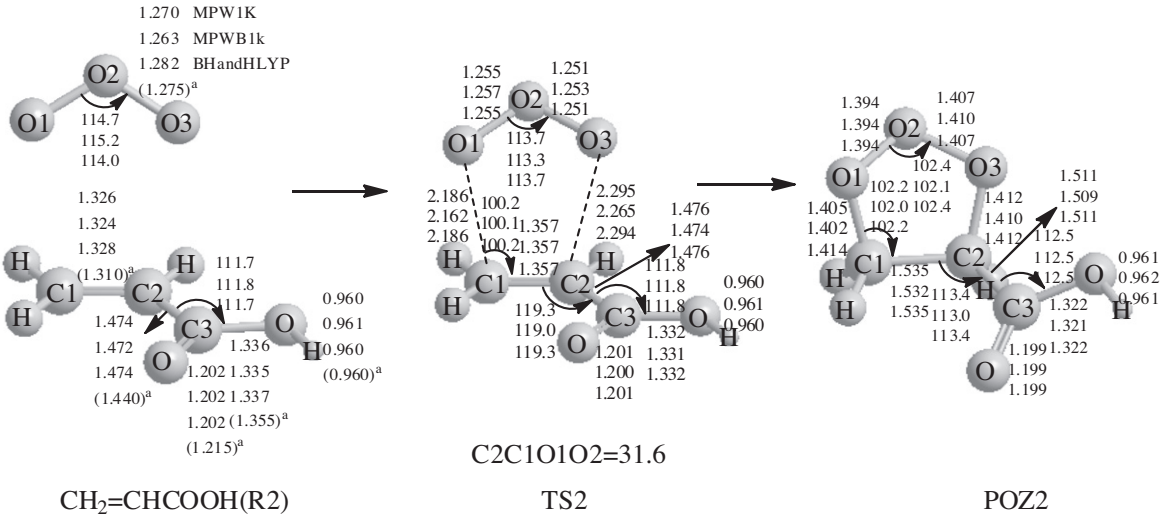

Fig. 2. Cycloaddition of ozone on acrylic acid: Optimized BH&HLYP, MPWB1K and MPW1K geometries of the stationary points. Angles are given in degree, and bond distances are given in angstroms. [a]Values in parentheses are from the experimental values [50].

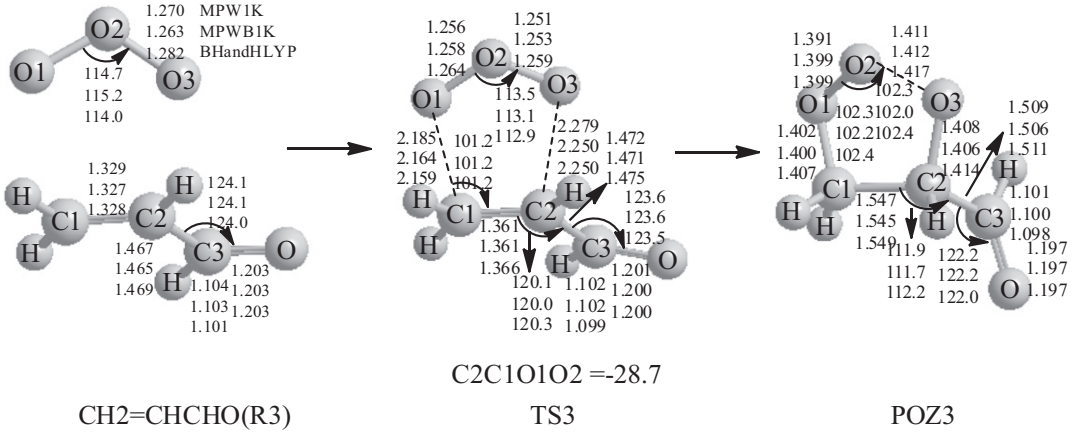

Fig. 3. Cycloaddition of ozone on allyl aldehyde: Optimized BH&HLYP, MPWB1K and MPW1K geometries of the stationary points. Angles are given in degree, and bond distances are given in angstroms.

function (per unit volume for bimolecular). Translational and rotational partition functions are evaluated classically, whereas the vibrational partition functions are calculated quantum mechanically within the harmonic approximation for the present studies. The SCT tunneling method [29–31] was employed to calculate the transmission coefficient in the calculation of the CVT rate constant.

The micro canonical variational transition state theory (μVT) [25,32,33] is based on the idea by minimizing the micro canonical rate constants along the MEP, one can minimize the error caused by the "recrossing" trajectories. Within the framework of μVT, the rate constant at a fixed temperature T can be expressed as:

$$k^{\mu VT}(T) = \frac{\int_0^{\infty} \min\{N^{GTS}(E,s)\} e^{-E/k_B^T} dE}{h\Phi^R}$$

where Φ^R is the total reactant partition function, which is the product of electronic, rotational, and vibrational partition functions. The relative translational partition function is calculated classically, and is included in Φ^R. However, the rotational and vibrational partition functions of the reactant are calculated quantum mechanically within the rigid rotor and harmonic oscillator approximations, respectively. $N^{GTS}(E,s)$ is the sum of states of electronic, rotational, and vibrational motions at energy E of the generalized transition state located at s, where s is the reaction coordinate.

3. Results and discussion

3.1. Reaction of ozone with allyl alcohol (Reaction 1)

We present a direct ab initio and density functional theory study of the thermal rate constants of the cycloadditions of ozone to allyl alcohol. BH&HLYP, MPWB1K, and MPW1K levels of theory with the 6-31 + G(d,p) basis set are employed to optimize the geometries and frequencies of all the stationary points and to calculate the MEP. The rate constant calculations are carried out with energies obtained by the BH&HLYP/6-31 + G(d,p), MPWB1K/6-31 + G(d,p), MPW1K/6-31 + G(d,p) and CCSD(T)/6-31 + G(df,p) levels of theory. Among all methods, the calculated rate constants at the BH&HLYP/6-31 + G(d,p) level of theory are in good consistent with experimental data. For example, the TST rate constants of the Reaction 1 at 298 K is 1.14×10^{-17} cm^3 mol^{-1} s^{-1} and the experimental standard [44] rate constants is $(1.44 \pm 0.2) \times 10^{-17}$ cm^3 mol^{-1} s^{-1} at (298 ± 3)K. The little difference between the theoretical and experimental standard rate constants suggests that BH&HLYP is good for estimating the energies of current work.

The reaction of O_3 with alkenes has been shown to take place by electrophilic addition to the double-bond system to produce a primary ozonide [45,46,13]. The ozonolysis of allyl alcohol is more

similar to the ozonolysis of ethylene investigated by Gillies [47] and Cremer [48]. The most favorable reaction path passes through an O-envelope-shaped VDW complex and transition state, producing a primary ozonide of the same structure. During the early stages of the addition of ozone to allyl alcohol, a weakly bound VDW complex is formed. The calculated structural parameters for the complex are given in the Supporting Information (Fig. 1S). We consider various structures for these complexes, the most stable one lies in a shallow minimum 0.94 kcal/mol below the reactants at the BH&HLYP/6-31 + G(d,p) level of theory. The absolute energy of the complex with zero-point energy correction is −418.197338 kcal/mol. Since the VDW complex is of little importance for the observed reactivity, we will only discuss the DFT geometries for the latter two structures, which are characterized by this computational technique as stationary points on the potential energy surface. Graphical representations of the BH&HLYP transition structure and primary ozonide are depicted in Figs. 1–3, which also compare the bond distances and angles obtained for the different computational techniques. The calculated results of the three DFT methods indicate that the structures of TS1 resemble the O-envelope conformation. Also TS1 resembles the reactants very well, for example, the O–O bond distances of 1.259 Å is only marginally smaller than that in ozone. We can therefore conclude that the system reach its TS1 during the early stage of the cycloaddition. The imaginary frequency of 248i cm^{-1} (TS1) associated with the reaction coordinate involves the stretching of the bond between O1 and C1 atoms. The subsequent IRC calculation confirms that TS1 connects the reactants (R1) with the primary ozonide (POZ1). The C–O bond length decreases smoothly with the increase of the IRC coordinate. The C–O distances of the TS1 are between 2.264 and 2.327 Å, 0.859–0.908 Å longer than those of the corresponding POZ1. The step of the cycloaddition ends in the POZ1. The calculations indicate that the geometries of POZ1 also correspond to the oxygen envelope conformation. The geometric parameters for stable points obtained from different computational techniques are in good agreement with one another. The relative energies of R1, TS1, and POZ1 with respect to the reactants ozone and allyl alcohol calculated at BH&HLYP/6-31 + G(d,p) level of theory are shown in Fig. 4. Our calculated reaction barrier energy of the Reaction 1 is 2.92 kcal/mol and our computation produces the large exothermicity 71.90 kcal/mol. The small reaction barrier energy and the large reaction energy of reaction are similar to the corresponding value reported previously for the O_3–ethene reaction [49]. The rate constants are evaluated based on the energies from the BH&HLYP/6-31 + G(d,p) level of theory using TST, CVT/SCT, and μVT theory in the temperature range of 200–3000 K. Fig. 5(A) depicts the rate constants of Reaction 1 together with experimental data [44]. As can be seen in Fig. 5(A), the agreement between our theoretical results and experimental value is good. The fitted three-parameter Arrhenius expressions of the calculated TST, CVT/SCT and μVT rate constants of the Reaction 1 are $k^{TST}(T) = 1.84 \times 10^{12} T^{0.88} e^{(-38087.0/T)}$, $k^{CVT/SCT}(T) = 1.78 \times 10^{12} T^{0.88} e^{(-38100.0/T)}$ and $k^{\mu VT}(T) = 5.08 \times 10^{12} T^{0.71} e^{(-38298.9/T)}$, respectively.

In view of the foregoing, it is appropriate to use the same computational methodology for our study on the ozonolysis of acrylic acid and allyl aldehyde. As a final remark concerning this reaction, we mention that the three DFT methods give acceptable results for the geometries of all the stationary points. But the relative energies calculated at BH&HLYP/6-31 + G(d,p) level of theory are more accurate than those of the MPWB1K and MPW1K.

3.2. Reaction of ozone with acrylic acid (Reaction 2)

To the best of our knowledge the addition of ozone to acrylic acid has only been studied on the experimental basis [50]; no theoretical study has been reported in the literature so far. From preliminary calculation, it is deduced that the ozonolysis of acrylic acid proceeds along a concerted fashion. In this case the addition can occur on the unsaturated carbon bonds which is the preferred site for ozone addition. The reaction takes place through the saddle point TS2 described in Fig. 2, which is very similar to the TS1. The evaluation of the vibrational frequencies confirmed that the geometries reported here represent minima on the potential energy surfaces. For the transition state identified, the calculated vibrational frequencies contain only one imaginary component 318i cm^{-1}, confirming the first-order saddle point configuration.

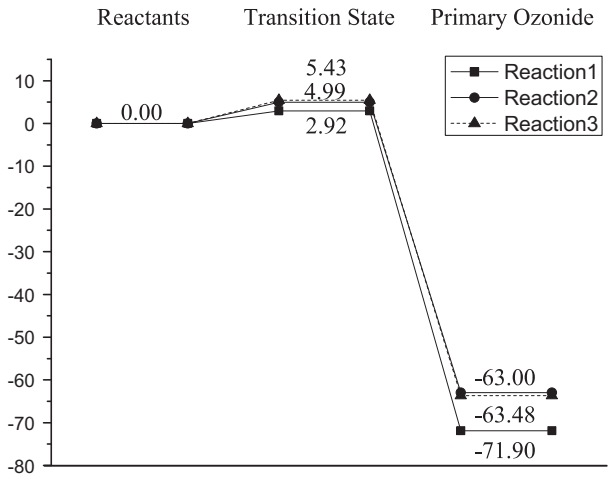

Fig. 4. Energy profile for the potential energy surface at the BH&HLYP/6-31 + G(d,p) level of theory. Relative energies are given in kcal/mol for all the stationary points. Zero-point energies (ZPE) corrections are included.

From Fig. 2, the results calculated in this work using the three DFT methods are consistent with the experimental values [51], especially for the geometrical parameters. The absolute errors of interatomic distances for all geometrical parameters are less than 0.03 Å. The C1–O1 and C2–O3 bonds are partially formed in TS2, while the C1–C2 bond is a little lengthened in TS2 with respect to that in R2. The C–O bonds at TS2 are in the range of 2.162–2.295 Å, which control the approach of the reactants. In view of electrostatic interaction, O_3 should approach to CH_2=CHCOOH in a non-symmetrical way with some preference toward the two carbon atoms. As a result the C1–O1 and as a result the C1–O1 distance (2.186 Å) is shorter than the C2–O3 distance (2.294 Å) in the BH&HLYP/6-31 + G(d,p) optimized TS2 structure. In the POZ2, the C1–O1 bond distances are reduced to 1.402–1.414 Å. The ∠C2C1O1O2 in TS1 and TS2 are 38.5° and 31.6° (Figs. 1 and 2), respectively. The conformation of TS1 is more contorted than transition state TS2. The difference could well be explained by the substituent effects.

As shown in Fig. 4, the barrier height is predicted to be 4.99 kcal/mol by BH&HLYP/6-31 + G(d,p) calculations. We propose 63.48 kcal/mol as our final estimate for the exothermicity of the Reaction 2. The barrier height of the Reaction 2 is larger than that of the Reaction 1; and the exothermicity of the Reaction 2 is smaller than that of Reaction 1. The reaction of ozonolysis of acrylic acid is predicted to be slower than the ozonolysis allyl alcohol reaction. Compounds with a –COOH functional group attached to the C=C reaction centre react slowly with ozone, reflecting the electron-withdrawing effect of the carboxylic acid group. The theoretical conclusion is confirmed by measured reaction rates [52,53]. Fig. 5(B) shows the Arrhenius plots vs. the temperatures. The rate constants obtained by experiment technique for the Reaction 2 at the temperature 298 K are also shown in Fig. 5(B) [52]. The calculated rate constant at BH&HLYP/6-31 + G(d,p) level of theory are in good agreement with the experimental data

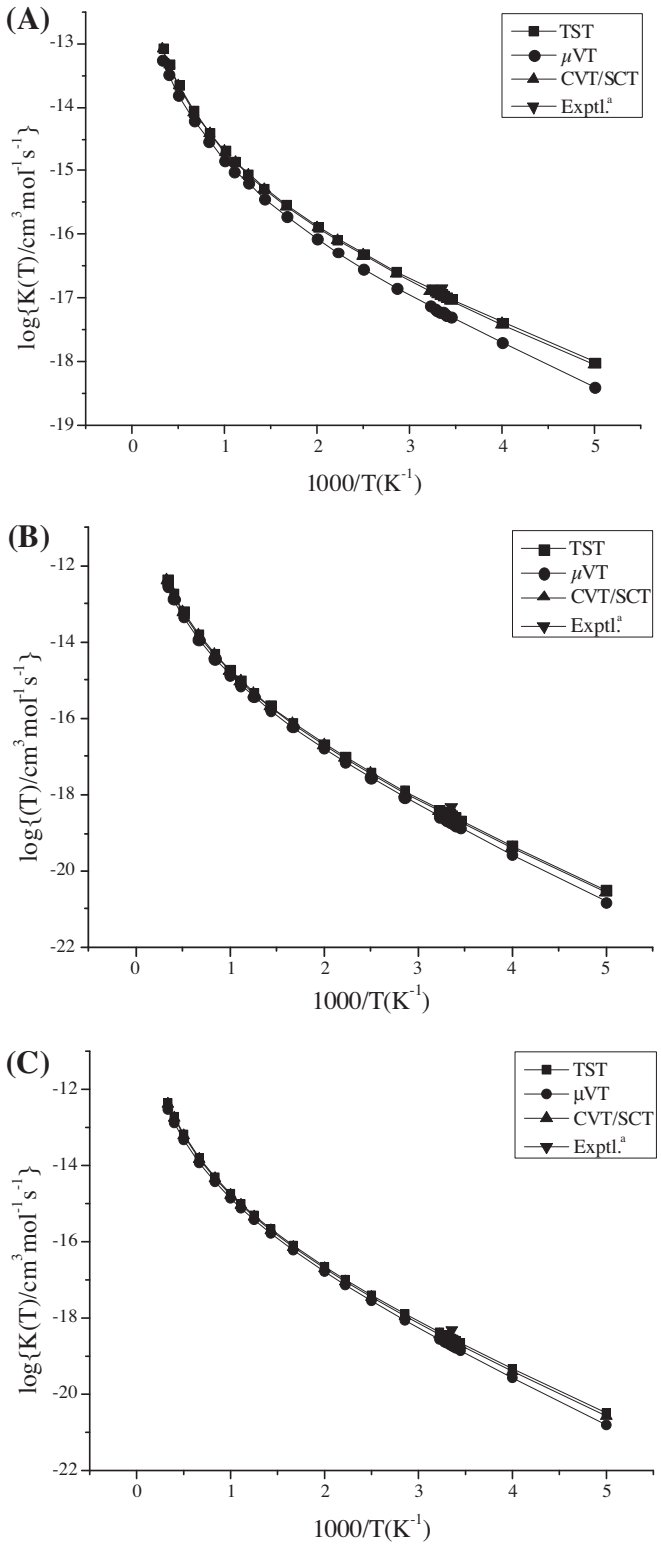

Fig. 5. Calculated Arrhenius plots of the rate constants at the BH&HLYP/6-31 + G(d,p) level of theory of the reaction vs. 1000/T(K^{-1}): (A) The reaction of ozone with allyl alcohol. (B) The reaction of ozone with acrylic acid. (C) The reaction of ozone with allyl aldehyde. [a]The experimental values from Refs. [44,51].

$(7.60 \pm 0.51) \times 10{-}19\ cm^3\ mol^{-1}\ s^{-1}$ at (298 ± 6) K. The fitted three-parameter Arrhenius expressions of the calculated TST, CVT and μVT, rate constants of the Reaction 2 are $k^{TST}(T) = 1.89 \times 10^{11} T^{0.84} e^{(-34468.6/T)}$, $k^{CVT/SCT}(T) = 1.89 \times 10^{11} T^{0.83} e^{(-34469.8/T)}$ and $k^{\mu VT}(T) = 1.04 \times 10^{12} T^{0.59} e^{(-34652.7/T)}$, respectively.

3.3. Reaction of ozone with allyl aldehyde (Reaction 3)

A pictorial of the optimized geometries and the calculated geometric parameters of the equilibrium and transition state of the cycloaddition of ozone to allyl aldehyde are displayed in Fig. 3. From the reactants (R3), the primary ozonide (POZ3) is finally reached through the transition state (TS3). Since the transition state leading to the primary ozonide is responsible for the overall reaction rate of the oxidation process, we will discuss the geometries for the transition state and primary ozonide. The TS3 is searched using constrained geometry optimization at fixed C–O bond lengths with BH&HLYP/6-31 + G(d,p). The lowest energy conformation of the POZ3 is illustrated in Fig. 3. We first consider the equilibrium structures of the POZ3 as the initial guess for the TS3. The two C–O bond lengths are then successfully increased by a fixed increment relative to the equilibrium C–O bond length of the POZ3. Once a transition state is located, the geometry is optimized at the BH&HLYP/6-31 + G(d,p) level of theory. The IRC carried out subsequently confirms the nature of TS3. For the transition state, the predicted geometries also agree well between all the levels of theory.

The C1–C2 bond length increases little from the reactants to the corresponding transition state (see Fig. 3). It is evident that the transition state has its structure close to the reactants. The length of the C–O bond in POZ3 decreases to 1.407 Å, with respect to the corresponding bond length of the transition state (2.159) at the BH&HLYP/6-31 + G(d,p) level of the theory. The stationary point TS3 has been characterized as a transition state with an imaginary frequency of 323i cm^{-1} that involves the contraction of the C–O bond. The ∠C2C1 O1O2 in TS3 is −28.7°. An effort to locate other isomers of the primary ozonide has been made and the most stable one (POZ3) has been found. As shown in Fig. 4, our reaction barrier energy (5.43 kcal/mol) of the Reaction 3 is larger than that calculated for the Reaction 2. Most probably the substitution of –CHO is responsible for the loss of reactivity, since the systems react in a mechanistically similar fashion. Our calculation arrives at an exothermicity of 63.00 kcal/mol, which corresponds to the large reaction energy (63.48 kcal/mol) for the Reaction 2.

For the Reaction 3, the fitted three-parameter Arrhenius expressions of the calculated TST, CVT and μVT, rate constants are $k^{TST}(T) = 1.90 \times 10^{11} T^{0.80} e^{(-35011.7/T)}$, $k^{CVT/SCT}(T) = 1.85 \times 10^{11} T^{0.80} e^{(-35010.3/T)}$ and $k^{\mu VT}(T) = 4.35 \times 10^{11} T^{0.64} e^{(-35170.7/T)}$, respectively. The curves of TST, μVT, and CVT nearly overlap in panels of Fig. 5(C), indicate that the variational effect on the calculation of rate constants are small and can be ignored. In Fig. 5(C), the TST rate constants are consistently slightly larger than the CVT and μVT rate constants in the calculated temperature regions. Our calculated TST rate constants for the reaction at 298 K is $1.05 \times 10^{-19}\ cm^3\ mol^{-1}\ s^{-1}$ and is in good agreement with experimental data $2.80 \times 10^{-19}\ cm^3\ mol^{-1}\ s^{-1}$ [51]. Comparing the rate constants reveals that the substitution of a –COOH group by a –CHO group leads to a decrease of the rate constants. This is in accordance with the basic concept of the Criegee-mechanism that the ozonolysis is initiated by a cycloaddition. According to our calculations, the ozone–acrylic acid reaction is slower than ozone–allyl alcohol reaction but faster than the ozone–allyl aldehyde reaction.

These results also can be rationalized in terms of the reduction in the electron density (ED) at the double bond due to the presence of the electron-withdrawing inductive effect of the carbonyl group. Thus, we perform a NBO analysis for the difference between NBO ED in the three primary ozonides and isolated reactants in O1–O2, C1–C2 sigma bonding and sigma antibonding orbitals to understand the properties of the interactions in the primary ozonides. The results are given in Table 1. The ED value in the C1–C2 sigma bonding orbital decreases a little, while it increases in the

Table 1
Charge transfer (CT,e), differences between NBO Electron Density in the primary ozonides and isolated reactants in O1–O2, C1–C2 sigma bonding ($\Delta\sigma$) and sigma antibonding ($\Delta\sigma^*$) orbitals are calculated at the BH&HLYP/6-31 + G (d,p) level.

	CT[a]	$\Delta\sigma_{O1-O2}$[b]	$\Delta\sigma^*_{O1-O2}$[b]	$\Delta\sigma_{C1-C2}$[b]	$\Delta\sigma^*_{C1-C2}$[b]
Allyl alcohol	−0.13911	−0.00826	0.00054	−0.01291	0.02334
	(−0.29880)	(1.98853)	(0.04351)	(1.97860)	(0.03220)
Acrylic acid	−0.13214	−0.00851	0.00031	−0.01253	0.02127
	(−0.29183)	(1.98828)	(0.04328)	(1.97637)	(0.02923)
Allyl aldehyde	−0.13205	−0.00863	−0.00074	−0.02518	0.02432
	(−0.29174)	(1.98816)	(0.04223)	(1.96640)	(0.03257)

[a] The charge transfer is obtained by subtracting the sum of atom charges on the electron acceptor molecule in the monomer from that in the primary ozonide. The natural charges of primary ozonides on O1 atom are enclosed in parentheses.
[b] The data in parentheses are the occupation numbers of the considered orbits in the primary ozonides.

corresponding antibonding orbital of each primary ozonide. The latter increase is much larger than the former decrease. The latter effect should be mainly responsible for the elongation of C1–C2 bond in the primary ozonides. Moreover, the charge transfer occurs between the two molecules. As shown in Table 1, the negative charge of O1 atom in the POZ1 is larger than that in the POZ2 and POZ3. The increased negative charge over oxygen atom enhances the interaction between the ozone and allyl alcohol. Therefore, we can draw a conclusion that the reaction of allyl alcohol with ozone proceeds easily. The results are in agreement with our analysis of the charge transfer.

4. Summary

In our paper, for discussing effects of substituent on the reactions, the cycloaddition reactions of the ozone with allyl alcohol, acrylic acid and allyl aldehyde have been studied with three different methods (BH&HLYP, MPWB1K and MPW1K). The geometric parameters for stable points obtained from different computational techniques are in good agreement with one another. The energetic information of all the point is further refined by the CCSD (T) method. The little difference between the theoretical and experimental standard rate constants suggests that BH&HLYP is better for estimating the energies of current work. The rate constants are evaluated based on the energies from the BH&HLYP/6-31 + G(d,p) level of theory using TST, CVT, and μVT theory in the temperature range of 200–3000 K.

The reactions of the ozone with allyl alcohol (Reaction 1), acrylic acid (Reaction 2) and allyl aldehyde (Reaction 3) show a similar mechanism, outlined as follows: from the reactants, the primary ozonides are directly reached through transition states (TS1, TS2 and TS3). The barrier heights for TS1, TS2 and TS3 are 2.92, 4.99, and 5.43 kcal/mol at the BH&HLYP/6-31 + G(d,p) level of theory, respectively. Furthermore, the most stable primary ozonides of allyl alcohol, acrylic acid and allyl aldehyde are calculated at 71.90, 63.48 and 63.00 kcal/mol below the corresponding entrance channels. Thus, we can conclude that for an addition of ozone to unsaturated oxygenated compounds with different functional groups has a distinct correlation between the barrier height and the extent of the exothermicity.

The extended Arrhenius expressions fitted from the TST, CVT/SCT and μVT rate constants of the Reaction 1 in the temperature range 200–3000 K are $k^{TST}(T) = 1.84 \times 10^{12} T^{0.88} e^{(-38087.0/T)}$, $k^{CVT/SCT}(T) = 1.78 \times 10^{12} T^{0.88} e^{(-38100.0/T)}$ and $k^{\mu VT}(T) = 5.08 \times 10^{12} T^{0.71} e^{(-38298.9/T)}$, respectively. The fitted three-parameter Arrhenius expressions of the calculated TST, CVT/SCT and μVT rate constants of the Reaction 2 are $k^{TST}(T) = 1.89 \times 10^{11} T^{0.84} e^{(-34468.6/T)}$, $k^{CVT/SCT}(T) = 1.89 \times 10^{11} T^{0.83} e^{(-34469.8/T)}$ and $k^{\mu VT}(T) = 1.04 \times 10^{12} T^{0.59} e^{(-34652.7/T)}$, respectively. For the Reaction 3, the fitted three-parameter Arrhenius expressions of the calculated forward TST, CVT/SCT and μVT rate constants are $k^{TST}(T) = 1.90 \times 10^{11} T^{0.80} e^{(-35011.7/T)}$, $k^{CVT/SCT}(T) = 1.85 \times 10^{11} T^{0.80} e^{(-35010.3/T)}$ and $k^{\mu VT}(T) = 4.35 \times 10^{11} T^{0.64} e^{(-35170.7/T)}$, respectively. By using arguments based on energetics and rate constants, the ozone–acrylic acid reaction is slower than ozone–allyl alcohol reaction but faster than ozone–allyl aldehyde reaction, consistent with the relative magnitude of the electron-withdrawing influence of the oxygenated substituent (–CH_2OH > –COOH > –CHO). It is anticipated that these thermodynamics and kinetics data can be used to establish the modeling and testing methodologies that could be applied to larger molecules or to the complete reaction kinetic schemes.

Acknowledgments

We gratefully thank the National Natural Science Foundation of China (Nos. 20773014 and 20933001), the Research Foundation of Education Bureau of Hebei Province (No. Z2011115), the 111 Project of China (No. B07012) and the Natural Science Foundation of Hebei Province (No. B2012105002) for their support of this work.

Appendix A. Supplementary data

Supplementary data associated with this article can be found, in the online version, at http://dx.doi.org/10.1016/j.chemphys.2013.01.005.

References

[1] J. Arey, A.M. Winer, R. Atkinson, S.M. Aschmann, W.D. Long, C.L. Morrison, Atmos. Environ. A 25 (1991) 1063.
[2] P.D. Goldan, W.C. Kuster, F.C. Fehsenfeld, S.A. Montzka, J. Geophys. Res. A 100 (1995) 25945.
[3] A. Guenther, P. Zimmerman, L. Klinger, J. Greenberg, G. Eins, K. Davis, W. Pollock, H. Westberg, G. Allwine, C. Geron, J. Geophys. Res. 101 (1996) 1345.
[4] G. König, M. Brunda, H. Puxbaum, C.N. Hewitt, S.C. Duckham, J. Rudolph, Atmos. Environ. 29 (1995) 861.
[5] B. Barlettaa, S. Meinardia, I.J. Simpsona, Atmos. Environ. 36 (2002) 3429.
[6] A.M. Winer, J. Arey, R. Atkinson, S.M. Aschmann, W.D. Long, C.L. Morrison, D.M. Olszyk, Atmos. Environ. A 26 (1992) 2647.
[7] S. Zhou, I. Barnes, T. Zhu, I. Bejan, T. Benter, J. Phys. Chem. A 110 (2006) 7386.
[8] H. Singh, Y. Chen, A. Standt, D. Jacob, D. Blake, B. Heikes, J. Snow, Nature 410 (2001) 1078.
[9] A. Mellouki, G. Le Bras, H. Sidebottom, Chem. Rev. 103 (2003) 5077.
[10] R. Atkinson, W.P.L. Carter, Chem. Rev. 84 (1984) 437.
[11] R. Atkinson, J. Phys. Chem. Ref. Data 26 (1997) 215.
[12] J.G. Calvert, R. Atkinson, J.A. Kerr, S. Madronich, G.K. Moortgat, T.J. Wallington, G. Yarwood, The Mechanisms of Atmospheric Oxidation of the Alkenes, Oxford University press, New York, 2000.
[13] D. Johnson, G. Marston, Chem. Soc. Rev. 37 (2008) 699.
[14] J.H. Seinfeld, S.N. Pandis, Atomospheric Chemistry and Physics, Wiley, New York, 2006.
[15] E. Grosjean, D. Grosjean, J. Atmos. Chem. 32 (1999) 205.
[16] R. Atkinson, J. Arey, Chem. Rev. 103 (2003) 4605.
[17] A.L. Holloway, J. Treacy, H. Sidebottom, A. Mellouki, V. Daële, G. Le Bras, I. Barnes, J. Photochem. Photobiol. A: Chem. 176 (2005) 183.
[18] D. Johnson, J.M. Andino, Int. J. Chem. Kinet. 33 (2001) 328.
[19] J. Noda, G. Nyman, S. Langer, J. Phys. Chem. A 106 (2002) 945.
[20] S.M. O'Donnell, H. Sidebottom, J.C. Wenger, A. Mellouki, G. Le Bras, J. Phys. Chem. A 108 (2004) 7386.
[21] S.M. Aschmann, P. Martin, E.C. Tuazon, J. Arey, R. Atkinson, Environ. Sci. Technol. 35 (2001) 4080.
[22] E. Grosjean, D. Grosjean, Int. J. Chem. Kinet. 28 (1996) 911.
[23] R. Criegee, Angew. Chem. 87 (1975) 765.
[24] R. Criegee, Angew. Chem. Int. Ed. 14 (1975) 745.
[25] D.G. Truhlar, B.C. Garrett, S.J. Klippenstein, J. Phys. Chem. 100 (1996) 12771.
[26] D.G. Truhlar, B.C. Garrett, Annu. Rev. Phys. Chem. 35 (1984) 159.
[27] D.G. Truhlar, B.C. Garrett, J. Chem. Phys. 84 (1987) 365.
[28] T.N. Truong, J. Chem. Phys. 100 (1994) 8014.
[29] Y.-P. Liu, G.C. Lynch, T.N. Truong, J. Am. Chem. Soc. 115 (1993) 2408.
[30] D.G. Truhlar, A.D. Isaacson, B.C. Garrett, in: M. Baer (Ed.), Theory of Chemical Reaction Dynamics, vol. 4, 1985, pp. 65.
[31] D.G. Truhlar, A.D. Isaacson, R.T. Skodje, B.C. Garrett, J. Phys. Chem. 86 (1982) 2252.
[32] B.C. Garrett, D.G. Truhlar, J. Phys. Chem. 83 (1979) 1079.
[33] W. Hase, Acc. Chem. Res. 31 (1998) 659.
[34] B.J. Lynch, P.L. Fast, M. Harris, D.G. Truhlar, J. Phys. Chem. A 104 (2000) 4811.

[35] C. Lee, W. Yang, R.G. Parr, Phys. Rev. B. 37 (1988) 785.
[36] A.D. Becke, J. Chem. Phys. 98 (1993) 1372.
[37] A.D. Becke, J. Chem. Phys. 104 (1996) 1040.
[38] C. Adamo, V. Barone, J. Chem. Phys. 108 (1998) 664.
[39] Y. Zhao, D.G. Truhlar, J. Phys. Chem. 108 (2004) 6908.
[40] W.T. Duncan, R.L. Bell, T.N. Troung, J. Comput. Chem. 19 (1998) 1039.
[41] A.E. Reed, L.A. Curtiss, F. Weinhold, Chem. Rev. 88 (1988) 899.
[42] M.J. Frisch et al., Gaussian 03 Revision B.04, Gaussian Inc., Pittsburgh, PA, 2003.
[43] S. Zhang, T. N. Troung, VKLab Version 1.0; University of Utah, Salt Lake City, USA, 2001.
[44] A. Le Person, G. Solignac, Phys. Chem. Chem. Phys. 11 (2009) 7619.
[45] R. Atkinson, W.P.L. Carter, Chem. Rev. 84 (1984) 473.
[46] R. Atkinson, J. Phys. Chem. Ref. 26 (1997) 215.
[47] C.W. Gillies, J. Am. Chem. Soc. 99 (1977) 7239.
[48] D. Cremer, J. Am. Chem. Soc. 103 (1981) 3633.
[49] M.F.A. Hendrickx, C. Vinckier, J. Phys. Chem. A 107 (2003) 7574.
[50] R. Atkinson, S.M. Aschmann, A.M. Winer, J.N. Pitts, Int. J. Chem. Kinet. 13 (1981) 1133.
[51] N.A. Lange, Lange's Chemistry Handbook, 15th ed., Beijing World Publishing Corporation/McGraw-Hill, 1999.
[52] I. AlMulla, L. Viera, R. Morris, H. Sidebottom, J. Treacy, A. Mellouki, Chem. Phys. Chem. 11 (2010) 4069.
[53] D. Grosjean, E. Grosjean, E.L. Williams II, Int. J. Chem. Kinet. 25 (1993) 783.